



Article

Thermal Degradation Mechanism and Decomposition Kinetic Studies of Poly(Ethylene Succinate)/Hemp Fiber Composites

Iouliana Chrysafi ¹, Nina Maria Ainali ², Eleftheria Xanthopoulou ², Alexandra Zamboulis ²
and Dimitrios N. Bikiaris ^{2,*}

¹ Laboratory of Advanced Materials and Devices, Department of Physics, Faculty of Sciences, Aristotle University of Thessaloniki, 54124 Thessaloniki, Greece; iochrysa@physics.auth.gr

² Laboratory of Polymer Chemistry and Technology, Department of Chemistry, Faculty of Sciences, Aristotle University of Thessaloniki, 54124 Thessaloniki, Greece; nsainali@chem.auth.gr (N.M.A.); elefthxanthopoulou@gmail.com (E.X.)

* Correspondence: dbic@chem.auth.gr; Tel.: +30-2310-997812

Abstract: The continuous depletion of natural resources coupled with plastics pollution, has prompted the scientific community to explore alternative biobased and/or biodegradable polymers. Poly(ethylene succinate) (PESu) is a promising substitute due to its high processability and controllable biodegradation rate. Meanwhile, hemp possesses interesting properties such as being lightweight, exhibiting excellent long-term mechanical stability, and having low carbon emissions, making it an ideal option for wood replacement. Thus, PESu/hemp fiber composites (with and without compatibilizer) were prepared novel sustainable materials with improved properties. The present study aims to investigate the thermal degradation of PESu/hemp fiber composites. More specifically, thermogravimetric analysis (TGA) and pyrolysis-gas chromatography/mass spectrometry (Py-GC/MS) were employed to examine the degradation mechanism and identify decomposition products. The isoconversional methods of Vyazovkin and Friedman, as well as the model free methods, provided comparable results. Samples without compatibilizer were characterized by a two-step Cn autocatalytic mechanism, while those with compatibilizer showed a triple Cn mechanism. The main thermal degradation pathway of the composites was the β -hydrogen scission of the polymeric backbone. In conclusion, this study provides information about the thermal behavior of PESu/hemp fiber composites useful for their application as alternative “wood plastic composites (WPCs)”.

Keywords: poly(ethylene succinate); hemp fibers; composites; thermal degradation; decomposition; isoconversional methods; model free methods; Py-GC/MS; TGA; wood plastic composites



Citation: Chrysafi, I.; Ainali, N.M.; Xanthopoulou, E.; Zamboulis, A.; Bikiaris, D.N. Thermal Degradation Mechanism and Decomposition Kinetic Studies of Poly(Ethylene Succinate)/Hemp Fiber Composites. *J. Compos. Sci.* **2023**, *7*, 216. <https://doi.org/10.3390/jcs7060216>

Academic Editors: Xiangfa Wu and Oksana Zholobko

Received: 5 April 2023

Revised: 8 May 2023

Accepted: 17 May 2023

Published: 25 May 2023



Copyright: © 2023 by the authors. Licensee MDPI, Basel, Switzerland. This article is an open access article distributed under the terms and conditions of the Creative Commons Attribution (CC BY) license (<https://creativecommons.org/licenses/by/4.0/>).

1. Introduction

In recent years, the demand for eco-friendly and sustainable materials has grown exponentially due to the increasing global ecological problems, including fossil fuel depletion and the adverse impact of plastic waste on the environment. Recycling of synthetic plastics is a sustainable solution, but the mechanical properties of recycled polymers are generally lower than those of virgin polymers, limiting their use in high-end applications. One of the most promising projects in this context is the development of bioplastics, which are derived from renewable resources. Upon degradation, these polymers reduce their molecular weight while increasing their crystallinity [1–7]. The addition of natural fillers and additives can enhance the physical and mechanical properties of these materials [8].

Poly(n-alkylene succinate)s, or PnASs, are a class of aliphatic, biodegradable polyesters that have gained significant interest due to their environmentally friendly characteristics, including their biodegradability [9]. The most commonly studied PnASs are poly(ethylene succinate) (PESu), poly(propylene succinate) (PPSu), and poly(butylene succinate) (PBSu), with PESu being one of the most important members due to its satisfactory mechanical

properties and good thermal stability [10–12]. PESu can be synthesized by either ring-opening polymerization of succinic anhydride or by polycondensation of succinic acid and ethylene glycol, both of which can be derived from natural resources [2,13]. Compared to non-biodegradable polymers, PESu presents controllable biodegradation rates and high processability, making it a promising alternative to traditional plastics. Furthermore, its mechanical properties, such as elongation at break and tensile strength, are comparable to those of commonly used polymers like low-density polyethylene (LDPE) and polypropylene (PP) [14,15].

Wood is abundant and, as a material, it exhibits excellent mechanical properties and is biodegradable. Therefore, it is an ideal material for furniture, construction elements, etc. However, wood consumption has long been a major cause of environmental problems, including deforestation and depletion of natural resources. As a response, researchers and manufacturers have turned to the development of alternative materials, using biobased fillers [16], such as natural fiber reinforced plastics (NFRP) and “wood” plastic composites (WPC) [17]. This has resulted in a shift towards the use of agricultural residues, such as hemp fibers, to replace natural wood. Hemp fibers offer several advantages, including good specific mechanical properties, high toughness, and ease of processing [18].

The use of hemp fibers for alternative “WPCs” production is particularly attractive due to their great availability and low cost [19]. Hemp fibers are strong and stiff and have a great potential as composite reinforcing agents. They typically consist of approximately 74% cellulose, 14% hemicellulose, 5% lignin, 1% pectins, and 6% of other substances such as waxes [18], but composition can differ among different hemp varieties. Hemp fibers interact strongly with matrices with similar nature to PESu [20], as evidenced by force spectroscopy measurements [21]. Based on their interfacial adhesion with the matrix, hemp fibers have been preferred as fillers, in comparison to other plants, like kenaf or jute. Additionally, as interfacial adhesion is crucial for the properties of the final composites, various methods, such as fiber treatment or addition of compatibilizers, are used to further increase the interactions between both phases [18,22,23].

Hemp fiber reinforced composites have a wide range of applications, including indoor and outdoor furniture, manufacturing of automotive parts, building structures, and textile applications [22,24,25]. Scarponi C. and Messano M. [26] tested hemp fiber and e-glass composites as a replacement for steel in electronic racks in rotorcraft interiors. Interestingly, hemp fiber composites exhibited comparable performances to glass fiber ones, but with a lower environmental impact. Sathish et al. [27] studied the incorporation of hemp and coir fibers in ramie/polypropylene composites for biomedical applications; it was demonstrated that mechanical properties could be fine-tuned by the fiber kind and content. According to a review published by Ticoalu A. et al. [28] hemp fiber/polypropylene composites showed higher tensile strength than coir/polypropylene composites. Several studies have also been conducted on concrete reinforced with hemp fibers for the construction sector [29–31]. These studies showed that hemp concrete can reduce energy consumption, decrease relative humidity variations, and improve fire resistance while preventing crack propagation. According to Asim Shajzad [32], by applying appropriate surface treatment moisture absorption can be avoided, affording hemp fiber composites that exhibit better mechanical properties than corresponding glass fiber composites. These non-exhaustive examples clearly demonstrate the high potential of hemp fibers as reinforcing fillers.

Hemp fibers have been employed to reinforce various polymers such as polyethylene, polypropylene, poly(lactic acid) in alternative “WPCs” [16–18,33,34]. To the best of our knowledge, the present work is the first dedicated to poly(ethylene succinate)/hemp fiber composites. These new composite materials are intended to replace wood-plastic composites, often used in exterior applications. As aforementioned, PESu exhibits good thermal properties, making it suitable for a wide range of applications in the packaging, textile, and biomedical industries [2,35], as other structurally similar biodegradable polymers [36]. PESu has a melting point around 103–106 °C and can be easily processed through various molding and extrusion techniques [14]. When it comes to thermal degradation, PESu has

been shown to degrade at temperatures above its melting point, in two stages, involving chain scission of the polymer backbone, thus resulting in the formation of oligomers and monomers [14]. The degradation rate of PESu is influenced by various factors such as processing temperature and conditions, as well as the presence of catalysts or other additives. In general, higher temperatures and longer processing times lead to faster degradation. However, the addition of stabilizers can significantly improve the thermal stability of PESu and increase its lifespan.

The present work aims to study the thermal degradation of PESu-hemp fibers composites. The scope of this research was to study new biobased composite materials that can replace common wood-plastic composites, most often produced with LDPE, HDPE, PVC and wood. PESu and hemp fibers will provide a biodegradable and more sustainable solution, not only from the plastics side but also from the perspective of the forest's deforestation. During the preparation of composites, in order to improve the adhesion between the fibers and the polymer matrix, Joncryl ADR-4400 (JC) compatibilizer was used. Thermogravimetric analysis (TGA) was used in conjunction with pyrolysis-gas chromatography/mass spectrometry (Py-GC/MS) to provide more details about the degradation process. Py-GC/MS is a technique that offers comprehensive insights into the thermal degradation pathways of polymeric materials. Through close examination of the degradation mechanism and identification of the resulting decomposition products, it becomes possible to select and implement optimized strategies for controlling thermal stability. The effect of the compatibilizer on the degradation of the composites was also investigated. Although research on the thermal degradation kinetics of PESu has been reported [12,37,38], this is the first study on the thermal degradation kinetics of PESu-hemp fibers composites.

2. Materials and Methods

2.1. Materials

Succinic acid (purity $\geq 99.5\%$), ethylene glycol (anhydrous, 99.8%), titanium isopropoxide ($\text{Ti}(\text{iOPr})_4$) were used for the synthesis of poly(ethylene succinate) (PESu) and were purchased from Sigma-Aldrich (Saint Louis, MO, USA). The polymeric chain extender Joncryl ADR®4400, in the form of flakes was supplied by BASF (Ludwigshafen, Germany). It has an epoxy equivalent weight of 485 g/mol and an average molecular weight of 7100 g/mol. All other solvents and materials used were of analytical grade.

Hemp fibers were supplied by KANNABIO (Volos, Greece). The hemp stems were obtained as agricultural waste after harvesting the seeds and flowers. The stems were cut using an agricultural machine, leaving a 5 cm distance from the ground, and were left in the field for 3–5 days. They were then manually collected and stored until the individual components (fiber and wood) could be separated. The defibrillation of the hemp was done using a HurdMaster MD1000 Hemp Micro Decorticator.

2.2. Synthesis of Poly(ethylene succinate) (PESu) and Its Composites with Hemp Fibers

PESu was synthesized by the two-stage melt polycondensation process, as previously reported [39]. PESu and hemp fibers were dried at 60 °C under vacuum for 24 h prior to the melt mixing in order to remove the adsorbed moisture. PESu composites containing 20 and 50% wt. hemp fibers of 0.5 cm length and 40 μm average diameter were prepared by melt mixing in a Haake–Buchler Reomixer (model 600) with roller blades and a mixing head with a volumetric capacity of 69 cm^3 . During the mixing period, the melt temperature and torque were continuously recorded. In this case, a 5 min mixing at 135 °C with a torque speed of 30 rpm was used. The same process was followed for the preparation of compatibilized composites with 10, 20, 50 and 75% wt. hemp fibers content. In addition, Joncryl ADR®4400 was added in an amount of 1 % wt., based on the amount of hemp fibers.

2.3. Characterization Methods

2.3.1. Thermogravimetric Analysis (TGA)

The thermal properties of PESu, hemp and the PESu-hemp fiber composites were evaluated through thermogravimetric analysis using a Labsys Evo 1100 instrument. The analysis involved placing samples weighing 4 ± 0.5 mg in alumina crucibles and heating them from room temperature to 600 °C in a 50 mL/min flow of nitrogen gas, using heating rates of 5, 10, 15, and 20 °C/min. An empty alumina crucible was used as reference. Measurements were continuously recorded for the sample temperature, sample mass, its first derivative, and heat flow. The NETZSCH Kinetics Neo software (Netzsch, Wunsiedel, Germany) was employed to perform kinetic analysis of the thermal degradation process and calculate the values of the kinetic triplet, which include the activation energy (E_a), pre-exponential factor (A), and reaction model ($f(\alpha)$).

2.3.2. Pyrolysis–Gas Chromatography/Mass Spectrometry (Py–GC/MS)

For Py–GC/MS analysis of the prepared composites, a very small amount of each material was ‘dropped’ initially into the ‘Double-Shot’ EGA/PY 3030D Pyrolyzer (Frontier Laboratories Ltd., Fukushima, Japan) using a CGS-1050Ex (Fukushima, Japan) carrier gas selector. For pyrolysis analysis (flash pyrolysis) each sample was placed into the sample cup which afterwards fell free into the Pyrolyzer furnace. The pre-selected pyrolysis temperature was set at 450 °C corresponding to the end of the thermal degradation of the composite materials as resulted by TGA analysis, while the GC oven temperature was heated from 50 to 300 °C at 10 °C/min. Sample vapours generated in the furnace were split (at a ratio of 1/50), a portion moved to the column at a flow rate of 1 mL/min, pressure 53.6 kPa and the remaining portion exited the system via the vent. The pyrolyzates were separated using temperature programmed capillary column of a Shimadzu QP-2010 Ultra Plus (Tokyo, Japan) gas chromatogram and analyzed by the mass spectrometer MS-QP2010SE of Shimadzu (Tokyo, Japan). Ultra-ALLOY® metal capillary column from Frontier Laboratories Ltd. (Fukushima, Japan) was used containing 5% diphenyl and 95% dimethylpolysiloxane stationary phase, column length 30 m and column ID 0.25 mm. For the mass spectrometer, the following conditions were used: Ion source heater 200 °C, interface temperature 300 °C, vacuum 10^{-4} –100 Pa, m/z range 10–500 atomic mass unit (amu) and scan speed 10,000 amu/s. The ion gas chromatograms and spectra retrieved by each experiment were subjected to further interpretation through Shimadzu and Frontier post-run software.

3. Results

3.1. Thermogravimetric Analysis

The thermal degradation of PESu and hemp fibers (HF) was investigated by heating at 10 °C/min, under nitrogen atmosphere. Figure 1 displays the mass loss and derivative of mass loss (dTG) versus temperature curves of PESu and hemp fibers. As shown in Figure 1a, PESu starts to degrade at approximately 200 °C, with the maximum degradation rate at 402 °C. The dTG curves suggest that the decomposition takes place in one stage, although there might be a second overlapping stage from 300 °C to 370 °C, which will be further studied by kinetic analysis.

On the other hand, the thermal degradation of hemp fibers (Figure 1b) takes place in three stages. In the initial stage, which occurs between 25 °C and approximately 155 °C, the sample loses 5% of its mass due to the evaporation of moisture. During the second stage, from 156 °C to 466 °C, 65% of the initial mass is lost, mainly due to the degradation of hemicellulose, pectin, and cellulose, as well as a small amount of lignin. According to Dolca C. et al. [17], hemicellulose decomposition is estimated to occur in a temperature range of about 220 °C to 315 °C, while cellulose decomposition occurs from about 320 °C to 420 °C. Lignin decomposes mainly from 150–900 °C. On the other hand, Asimakidou T. et al. [40] state that the decomposition of hemicellulose and cellulose take place from 170 °C to 360 °C and 240 °C to 380 °C, respectively, while lignin decomposes over a broader temperature

range extending up to the end of the process. Thus, according to literature, it can be assumed that in the second degradation stage, the decomposition of the lignocellulosic contents take place simultaneously. The maximum degradation rate is observed at 335 °C. Finally, between 466 °C and 950 °C, the sample loses an additional 18% of its mass due to lignin degradation, while the remaining mass after the experiment corresponds to 12% of the initial mass, attributed to biochar formation.

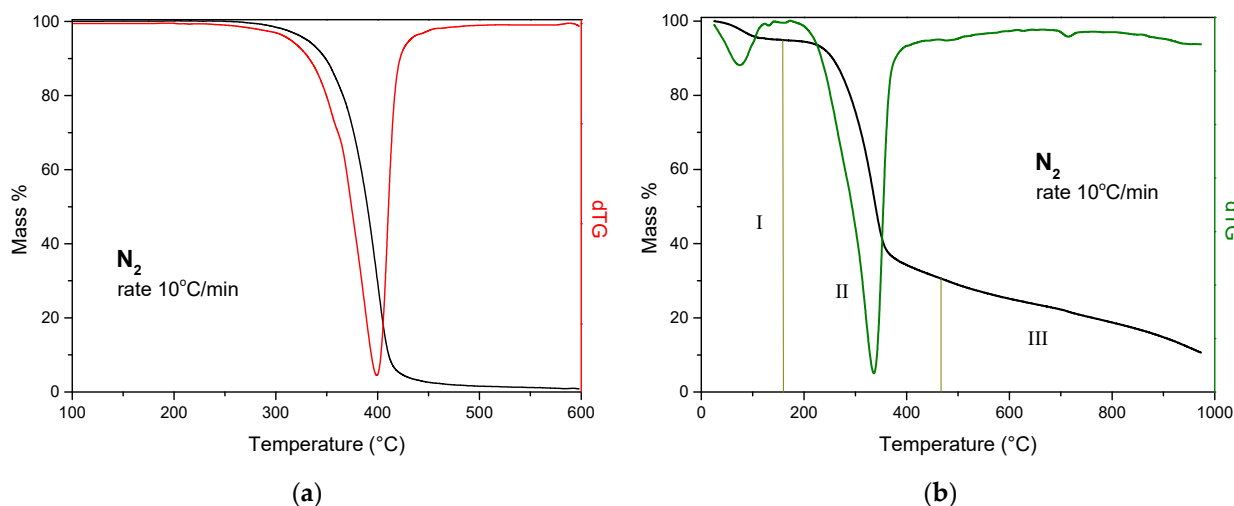


Figure 1. TGA thermograms of PESu (a) and hemp fibers (b). The continuous lines correspond to the mass % and the dashed lined to the dTG.

The following thermograms (Figure 2) compare PESu and PESu composites containing 20 and 50% wt. of hemp fibers, with and without the addition of the compatibilizer, heated at a rate of 20 °C/min. In the case of PESu (Figure 2a), both samples begin to degrade at approximately 270 °C. Compared to Figure 1a, degradation starts at higher temperatures due to the higher heating rate: the sample has less time to dissipate the heat, and so the temperature increases more quickly, providing more energy to break the chemical bonds. The maximum degradation rate of neat PESu is at 422 °C, while that of PESu + JC is at 432 °C. As for the composites with 20% wt. of hemp fibers (Figure 2b), the maximum degradation rate for both samples is at 405 °C, and degradation starts at approximately 260 °C, starting a few degrees lower in the sample without JC. In the case of the composite with 50% wt. of hemp fibers (Figure 2c), the degradation starts at approximately 205 °C, with the maximum degradation rate in the sample without JC at 395 °C and with JC at 400 °C. Two degradation steps are clearly visible, with the first step attributed to the presence of hemp. In all three comparative thermograms, an increase in the remaining mass due to hemp can be observed (*vide infra*), as well as a slight increase in all samples with the presence of JC. In the three comparative samples it can be observed that those with JC exhibit a slightly better thermal stability. JC acts as chain extender, in other words it increases the length of the polymeric chains, thereby increasing the molecular weight and, and, as a result, the thermal stability [41–44].

Figure 3 presents the mass % and dTG versus temperature curves of the PESu/hemp fiber composites with the addition of the compatibilizer. At first glance, from the mass loss versus temperature thermogram (Figure 3a), it can be seen that as the content of HF increases in the composites the degradation starts earlier and the remaining mass increases. The presence of HF is getting more visible as its concentration increases since a first degradation step appears between 220 and 320 °C. Moreover, the maximum degradation rate is shifted towards lower temperatures (Table 1). The remaining mass increases from 2.7% without HF to 19.8% with 75% wt. of HF and corresponds to lignin which partially decomposes until 600 °C.

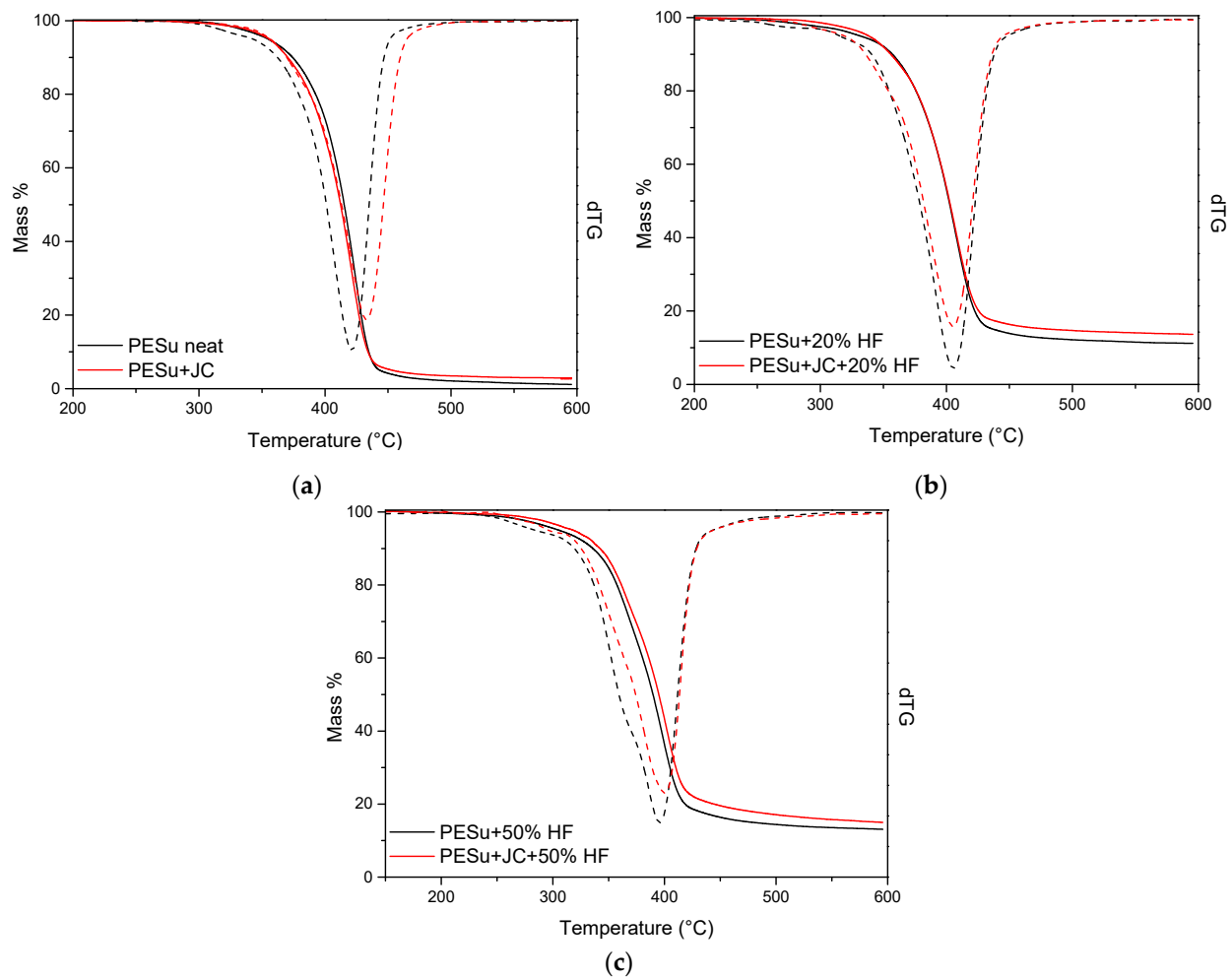


Figure 2. Comparative TGA thermograms of (a) PESu, (b) PESu + 20% wt. hemp fibers (HF), and (c) PESu + 50% wt. HF, with and without the presence of the compatibilizer. Heating rate: 20 °C/min.

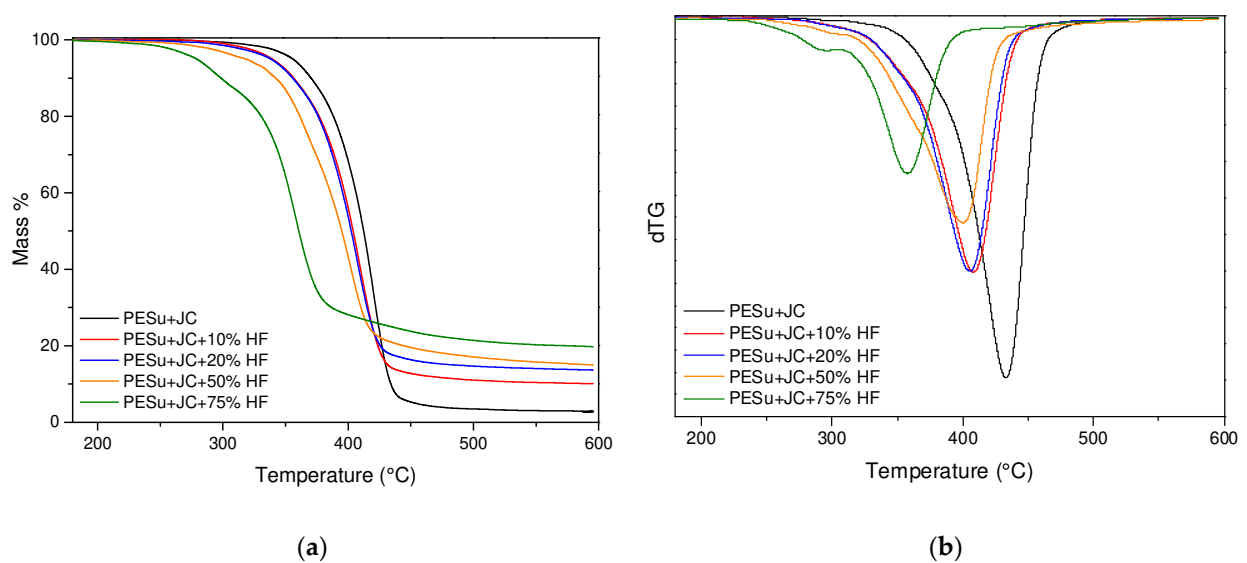
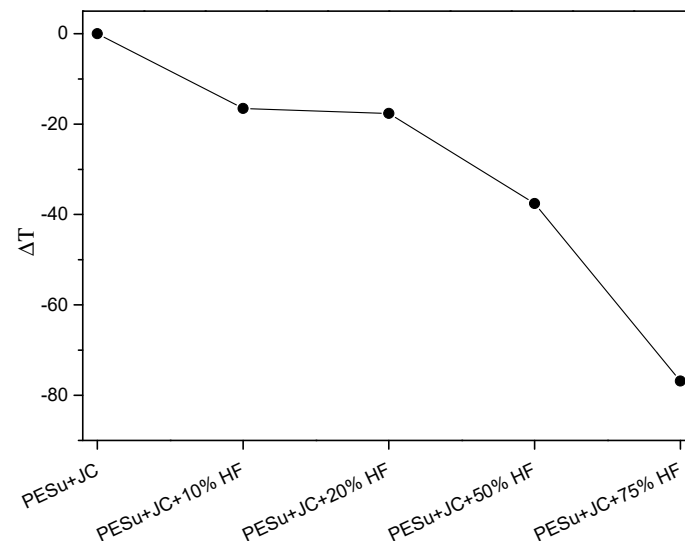


Figure 3. TGA thermograms of the mass loss (a) and derivative of mass loss (b) the PESu-hemp fiber composites with the presence of the compatibilizer under the heating rate of 20 °C/min.

Table 1. Temperatures of the maximum degradation rate of the first and the second steps and the remaining mass after each measurement.

Sample	Td ₁ (°C)	Td _{2,max} (°C)	Remaining Mass %
PESu + JC	-	433.6	2.7
PESu + JC + 10% HF	-	408.2	10.1
PESu + JC + 20% HF	299.8	405.5	13.7
PESu + JC + 50% HF	297.3	400.2	14.9
PESu + JC + 75% HF	289.9	357.5	19.8

The thermal stability (5% mass loss) of the samples was calculated taking PESu + JC as a reference (Figure 4). As observed in the mass loss thermogram, the thermal stability of the samples decreases with the increase of the HF content. This is expected due to the early start of the hemp fibers' decomposition. Therefore, the increase in HF content leads to the earlier initiation of the degradation and thus lower thermal stability. Although the difference between PESu and the composite with 75% HF is approximately 80 °C, this decrease does not significantly affect the use of these materials as WPCs, as the decomposition starts well above 200 °C.

**Figure 4.** Thermal stability of the composites compared to PESu with the presence of the compatibilizer.

3.2. Kinetic Analysis Based on Thermogravimetric Data—Isoconversional Methods

Kinetic analysis of the thermal degradation is a powerful tool used to understand degradation mechanisms and analyze thermal degradation processes. This can be achieved through thermogravimetric analysis (TGA), where kinetic analysis is used to accurately calculate the activation energy ($E\alpha$), pre-exponential factor (A), and the reaction mechanism ($f(\alpha)$) as a function of the degree of conversion (α). Kinetic analysis is carried out through two steps: isoconversional analysis and model fitting. Isoconversional methods have a significant role in the study of thermal degradation kinetics as they enable researchers to monitor the changes in the rate of degradation reactions over time, and to determine the activation energy and the pre-exponential factor. Model fitting methods identify the reaction mechanism and determine $E\alpha$ and A , resulting in more accurate outcomes [45]. The integral isoconversional method by Ozawa, Flynn, Wall (OFW), the differential isoconversional method by Friedman, and the integral isoconversional method of Vyazovkin, which has recently gained popularity [46,47], are among the most commonly used kinetic analysis methods for thermal analysis. The mechanisms of polymers degradation reactions are complex and involve various reactions including initiation, propagation, and termination [48]. Thus, the kinetic study of their degradation can provide useful information.

Isoconversional methods are referred to as "model-free" methods as they assume that the conversion function $f(\alpha)$ remains constant despite variations in the heating rate for the entire range of the degree of conversion α . Kinetic methods used in kinetic analysis consider the rate of the degree of conversion α as a function of two variables.

$$\frac{d\alpha}{dt} = k(T)f(\alpha) \quad (1)$$

where t is the time, T is the temperature, $k(T)$ is the rate coefficient originating from the Arrhenius law $k(T) = Ae^{-E_\alpha/RT}$, α is the degree of conversion and $f(\alpha)$ is the mathematical function denoting the reaction mechanism. In the Arrhenius law, A is the pre-exponential factor, T is the absolute temperature in Kelvin, E_α is the activation energy for the reaction and R is the universal gas constant. Equation (1) expresses the rate of conversion, $d\alpha/dt$, at a constant temperature as a function of the reactant mass loss and rate constant. The degree of conversion α is defined as:

$$\alpha = \frac{m_o - m_t}{m_o - m_f} \quad (2)$$

where m_t , m_o and m_f are the mass of the sample at the time t , the initial and the final condition, respectively.

The combination of the Arrhenius law and Equation (1), introducing the heating rate $\varphi = dT/dt$ for a dynamic TGA process gives the following equation:

$$\frac{d\alpha}{dT} = \frac{A}{\varphi} e^{-E_\alpha/RT} f(\alpha) \quad (3)$$

Integration of Equation (1) leads to:

$$g(a) = \int_0^a \frac{d(a)}{f(a)} = A \int_0^t e^{-E_\alpha/RT} dt \quad (4)$$

Integral isoconversional methods derive from the application of the isoconversional principle to the integral equation (Equation (4)). As the ICTAC Kinetics Committee [46] suggested, adding some rearrangements to Equation (4), the Ozawa, Flynn and Wall equation can be presented as:

$$\ln(\varphi_i) = \text{Const} - 1.052 \left(\frac{E_a}{RT_a} \right) \quad (5)$$

where $\varphi = dT/dt = \text{const}$ is the heating rate. The index i expresses the different heating rates that were applied on the experimental data. The values of the activation energy E_α can be obtained by the slope of the $\ln(\varphi_i)$ vs. $1/T_\alpha$ plots.

Vyazovkin has developed an advanced integral isoconversional method by dividing the integral form of equation 1 by the heating rate φ . This method deals with kinetics that take place under arbitrary variation in the temperature [49,50]. The activation energy can be determined for any given value of α in a series of n experiments conducted under different temperature programs $T_i(t)$, by minimizing the function to find E_α :

$$\Phi(E_\alpha) = \sum_{i=1}^n \sum_{j \neq i}^n \frac{J[E_\alpha, T_i(t_\alpha)]}{J[E_\alpha, T_j(t_\alpha)]} \quad (6)$$

where

$$J[E_\alpha, T_i(t_\alpha)] = \int_{t_\alpha - \Delta\alpha}^{t_\alpha} e^{-E_\alpha/RT_i(t)} dt \quad (7)$$

In Equation (6), the subscript α represents the values at a specific degree of conversion, which varies from $\Delta\alpha$ to $1 - \Delta\alpha$ with a step of $\Delta\alpha = m - 1$, where m is the number of

selected integrals. The minimization process is performed for each α value to obtain the E_α dependency on the degree of conversion.

Friedman's method is the most common differential isoconversional method that can be obtained by applying the isoconversional principle to Equation (1). Therefore, Friedman's equation is expressed as follows:

$$\ln \left[\varphi_i \left(\frac{d\alpha}{dT} \right)_{\alpha,i} \right] = \ln[f(\alpha)A_\alpha] - \frac{E_\alpha}{RT_{\alpha,i}} \quad (8)$$

where A is the pre-exponential factor and φ is the heating rate. To determine the activation energy E_α values, when the conversion function is constant, it is necessary to calculate the slope of the straight lines in the plot $\ln[\varphi_i(d\alpha/dT)_{\alpha,i}]$ versus $1/T_{\alpha,i}$. This involves taking temperature measurements that correspond to fixed α values at various heating rates φ . If the calculated activation energy remains consistent throughout the entire range of the degrees of conversion α , a single-step reaction can be established with certainty. The experimental data must be accurate for the kinetic study and identification of the mechanism or mechanisms of a transformation to yield useful results.

Kinetic analysis was performed on neat PESu and on the composite material with 20% wt. hemp fibers, both with and without the presence of the compatibilizer. The composite with 20% wt. of hemp fibers was chosen to evaluate the effect with and without JC. Furthermore, since the mass loss curves of the composite with 10% wt. of hemp fibers are similar to those of PESu, and the effect of hemp fibers becomes very significant at higher concentrations, resulting in a particularly complex curve, which, in turn, causes significant uncertainties in the kinetics, a medium concentration was chosen to provide the most accurate results. The isoconversional methods of Friedman and Vyazovkin were applied to the results. Figure 5 shows the activation energy (E_α) and the pre-exponential factor ($\log A$) as a function of the degree of conversion α . In general, both methods provide quite similar results, and the activation energy increases with the increase of the degree of conversion.

Neat PESu (Figure 5a) exhibits an increase in E_α from 100 to 140 kJ/mol until $\alpha = 0.9$, but above 0.9 a rapid increase follows until 180 kJ/mol. This indicates the possibility of more than one mechanism involved in the degradation process. On the contrary, the PESu sample with the addition of JC (Figure 5c) shows an initial rapid increase from 75 to 100 kJ/mol until $\alpha = 0.1$, then it increases linearly and above $\alpha = 0.8$ a second rapid increase follows from 140 to 185 kJ/mol. In this case as well, multiple mechanisms are indicated. Comparing the two PESu samples the one with JC varies across a wider energy range.

Quite the same behavior is observed for the composites with 20% of HF. A rapid increase in E_α is observed for PESu+20% HF above $\alpha = 0.8$, while for PESu + JC + 20% HF sample, two rapid increase stages are spotted: one at the beginning and one at the end. The activation energy ranges between 60 and 260 kJ/mol, while in the sample without JC from approximately 100 to 190 kJ/mol. The pre-exponential factor follows the same trend as E_α . Generally, the increase in the activation energy and in the pre-exponential factor with the increase in the degree of conversion suggests that the degradation reaction becomes more difficult to initiate and progresses more slowly as the reaction proceeds.

Subsequently, to determine the mechanisms involved in these processes, and to confirm the number of reactions that arise from kinetic analysis, "model fitting" was applied. It involves fitting different models to the experimental data and comparing them to the theoretical data, while determining the activation energy E_α and the pre-exponential factor A . The most commonly used reaction models for polymer thermal degradation are the n th-order model and the first-order model, because primarily these models are the simplest mathematical equations that can be used for identification.

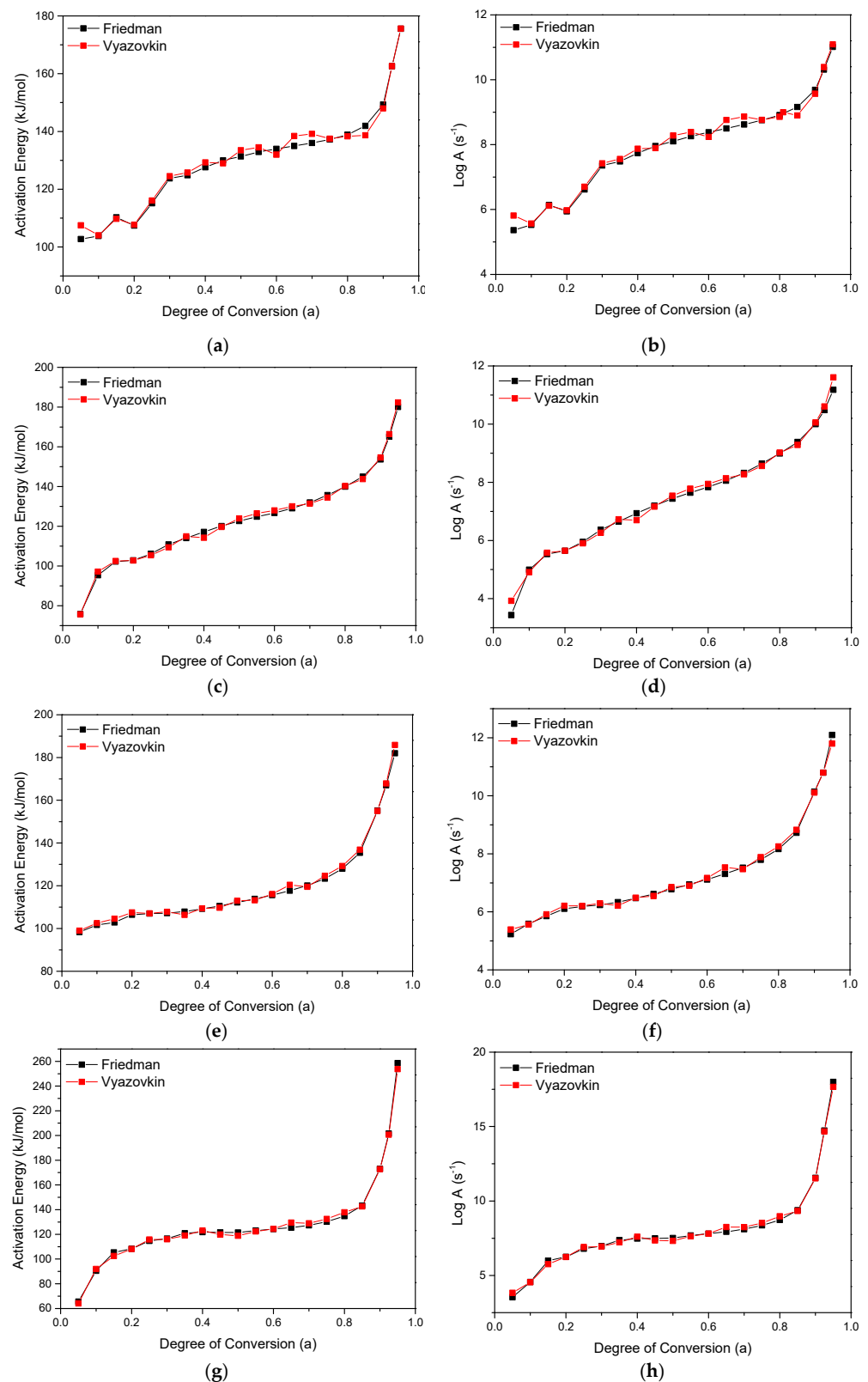


Figure 5. (a) Dependence of the activation energy (E_α) and (b) $\text{Log}(A)$ on the degree of conversion as calculated using the methods of Friedman and Vyazovkin for neat PESu (a,b), PESu + JC (c,d), PESu+20% HF (hemp fibers) (e,f) and PESu + JC + 20% HF (g,h). The average coefficient regression (R^2) of the Friedman method was 0.9999 and of the Vyazovkin method was 0.9998.

Therefore, to determine the thermal behavior of PESu and the composites with 20% wt. HF with and without JC, they were heated under the rates of 5, 10, 15 and 20 °C/min and the resulting data were fitted with 16 different kinetic models and their combinations. The initial assumption is that the degradation of the samples can be described by a single-step mechanism. However, if the fitting results do not meet the accepted criteria, it is mandatory to perform the experimental fitting with a combination of two or more mechanisms.

Kinetics Neo software was used in order to evaluate the experimental data. It is a useful tool that can analyze experimental data by using 16 different equations to identify the mechanism involved. This can be done either as a single mechanism or as a combination of different mechanisms. Due to the large number of equations and parameters available in the software, there can be numerous combinations that yield satisfactory results. Therefore, it is important to ensure that the correlation coefficient R^2 is very high, ideally around 0.999.

The single step procedure was initially applied to the 4 samples. As expected from the isoconversional methods none of them was accurately fitted with a single mechanism. Therefore, a second and a third mechanism were applied. Neat PESu and PESu + 20% HF (Figure 6a,c) were successfully fitted by a two-step mechanism, which included the nth order model with autocatalysis Cn: $f(\alpha) = (1 - \alpha)^n(1 + K_{cat})X$, where X is the extent of conversion of the autocatalytic reactions and K_{cat} is the autocatalysis rate constant. PESu with the presence of the compatibilizer as well as the PESu + JC + 20% HF sample were fitted with a triple step mechanism. In all cases the model was the nth order model with autocatalysis Cn.

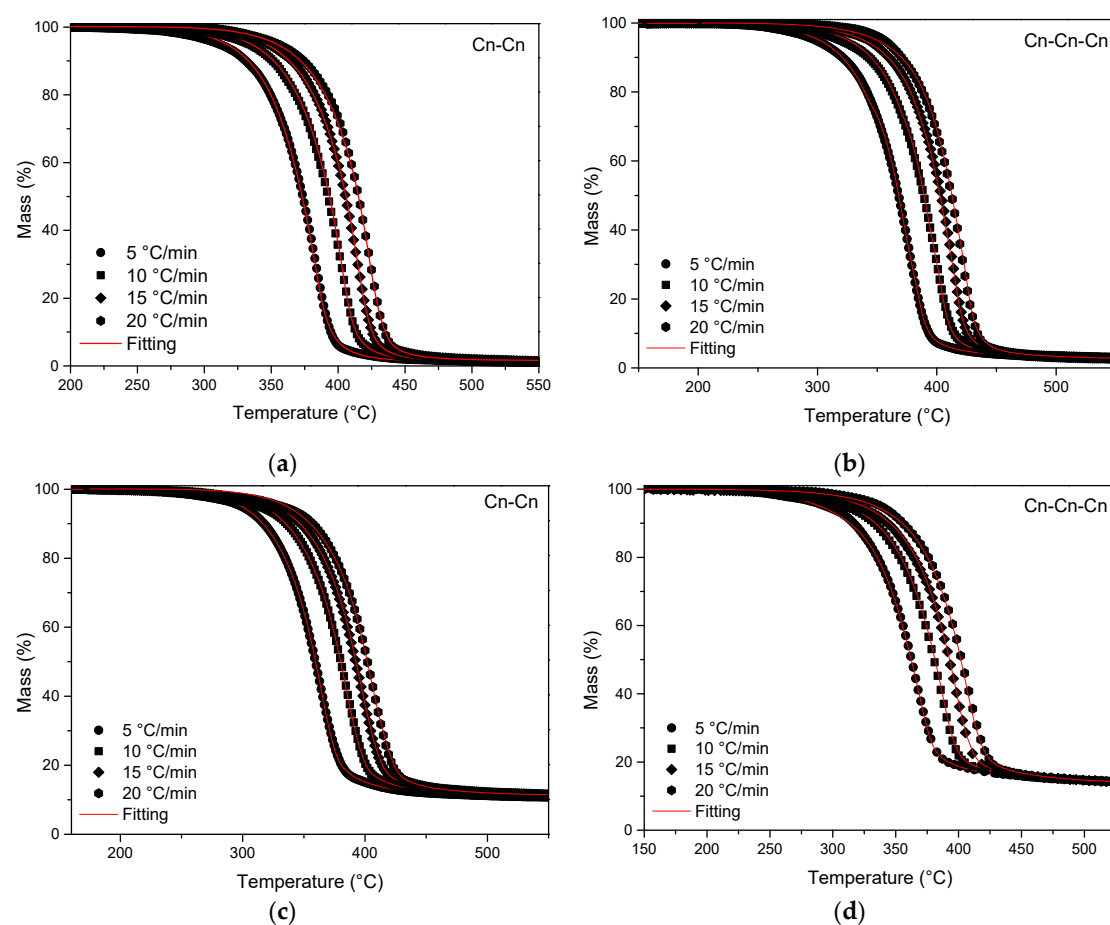


Figure 6. Thermal degradation of (a) neat PESu, (b) PESu + JC, (c) PESu + 20% hemp fibers (HF), and (d) PESu + JC + 20% HF, at different heating rates (circle) 5 °C/min, (square) 10 °C/min, (rhombus) 15 °C/min, (hexagon) 20 °C/min. The black symbols represent the experimental data, while the continuous red lines represent the fittings with different models.

Table 2 presents the calculated autocatalysis values of activation energy (E_a), pre-exponential factor (A), reaction order (n), branching rate constant (K_{cat}) and correlation coefficient (R^2) of the samples. As seen the fitting process was accomplished very accurately $R^2 > 0.9999$. In conclusion, it can be observed that the values of E_a and $\log A$ obtained from the “model fitting method” (Table 2) fall within the same range and follow the same trend as those obtained from the isoconversional methods of Friedman and Vyazovkin (Figure 5). The addition of JC results in the emergence of an initial region for low degrees of conversion ($\alpha < 0.3$), in which E_a significantly increases to 75 and 65 kJ/mol for PESu + JC and PESu + JC + 20% HF, respectively. The E_a values of the second step of the neat PESu and the third step in the PESu + JC sample remain similar. In contrast, in the composite with JC, E_a significantly increases from 180 kJ/mol (PESu + 20% HF) to 246 kJ/mol (PESu + JC + 20% HF). The addition of 20% wt. of HF without JC does not appear to affect the decomposition mechanisms of PESu: a two-step mechanism is observed for both and the E_a values are close. Therefore, the behavior of the PESu + JC + 20% HF sample, including both the number of degradation steps and the value of E_a in the third mechanism, seem to be caused by the presence of JC in the sample.

Table 2. Calculated autocatalysis values of activation energy (E_a), pre-exponential factor (A), reaction order (n), branching rate constant (K_{cat}) and correlation coefficient (R^2) of neat PESu, PESu + JC, PESu+20% HF (hemp fibers) and PESu + JC + 20% HF.

Sample	Step	Mechanism	E_a (kJ/mol)	$\log A$ (s^{-1})	$\log K_{cat}$	React. Order n	R^2
PESu	1st	Cn	107	6	0.3	0.6	0.99994
	2nd	Cn	170	10.7	1.2	2.1	
PESu + JC	1st	Cn	75	3.6	0.1	0.3	0.99994
	2nd	Cn	114	6.4	0.8	0.8	
	3rd	Cn	172	10.5	1.9	3.2	
PESu + 20% HF	1st	Cn	102	5.6	0.01	0.6	0.99992
	2nd	Cn	180	12.7	0.4	3.1	
PESu + JC + 20% HF	1st	Cn	65	3.2	0.01	1.1	0.99994
	2nd	Cn	123	0.7	0.01	0.7	
	3rd	Cn	246	17.6	0.9	4.2	

3.3. Pyrolysis–Gas Chromatography/Mass Spectrometry (Py–GC/MS) Study

Although TGA analysis provides general conclusions for the decomposition mechanism of the studied samples, Py–GC/MS delivers thorough data about the thermal degradation pathways of polymeric materials. Thermal degradation can alter the final performance and properties of a material, including its mechanical strength, thermal stability, and flammability. Thus, the detailed evaluation of the thermal degradation mechanism can assist in the choice of the optimal processing conditions or fillers required to control and ameliorate the thermal stability, while the behavior of already existing materials under different conditions can be predicted. Additionally, evaluating the thermal degradation pathway can help in terms of sustainability, since the thermal degradation mechanism can affect the recyclability, either directly or indirectly, and the biodegradability of the material. After investigating the thermal degradation mechanism of the materials, researchers can design materials with tunable recycling or biodegradable character.

Thermally induced degradation of polyesters has been extensively investigated since they hold a prominent role in the plastics market in comparison with other commodity polymers [51]. Concerning the main degradation pathway for carboxylic esters, it consists of a β -hydrogen transfer rearrangement, provoking the formation of vinyl esters and carboxylic acid end groups [10,21,37,52–56]. In detail, esters bearing at least one β -hydrogen decompose initially via a six-membered transition state over ester bonds to provide a pair of a carboxylic acid and olefinic segments. Succinic anhydride formation could be also favored, through cyclization degradation mechanism from succinic acid end groups, whether

already existing in the polymeric chains or formed throughout β -hydrogen bond scission reactions. In a further step, carboxyl end groups or larger molecules could decompose through decarboxylation, owing to the pyrolysis high temperatures, to form alkyl-ended fragments. Secondary mechanisms that take place mainly at higher temperatures (retention times) are the α -scission reactions and several homolytic processes.

Herein, the decomposition products of neat PESu and PESu/hemp fiber composites were analysed utilizing a Py-GC/MS instrumentation. All composites were pyrolyzed at 450 °C and the recorded total ion chromatographs (TICs) of the degradation products are presented in Figure 7. The aforementioned temperature was chosen since it is well above the $T_{d,max}$, as calculated from TGA measurements (Table 1). The most significant pyrolysis products were identified through their MS spectra and are presented in Table 3. Peak areas (%) were calculated with respect to the sum of the area of all components.

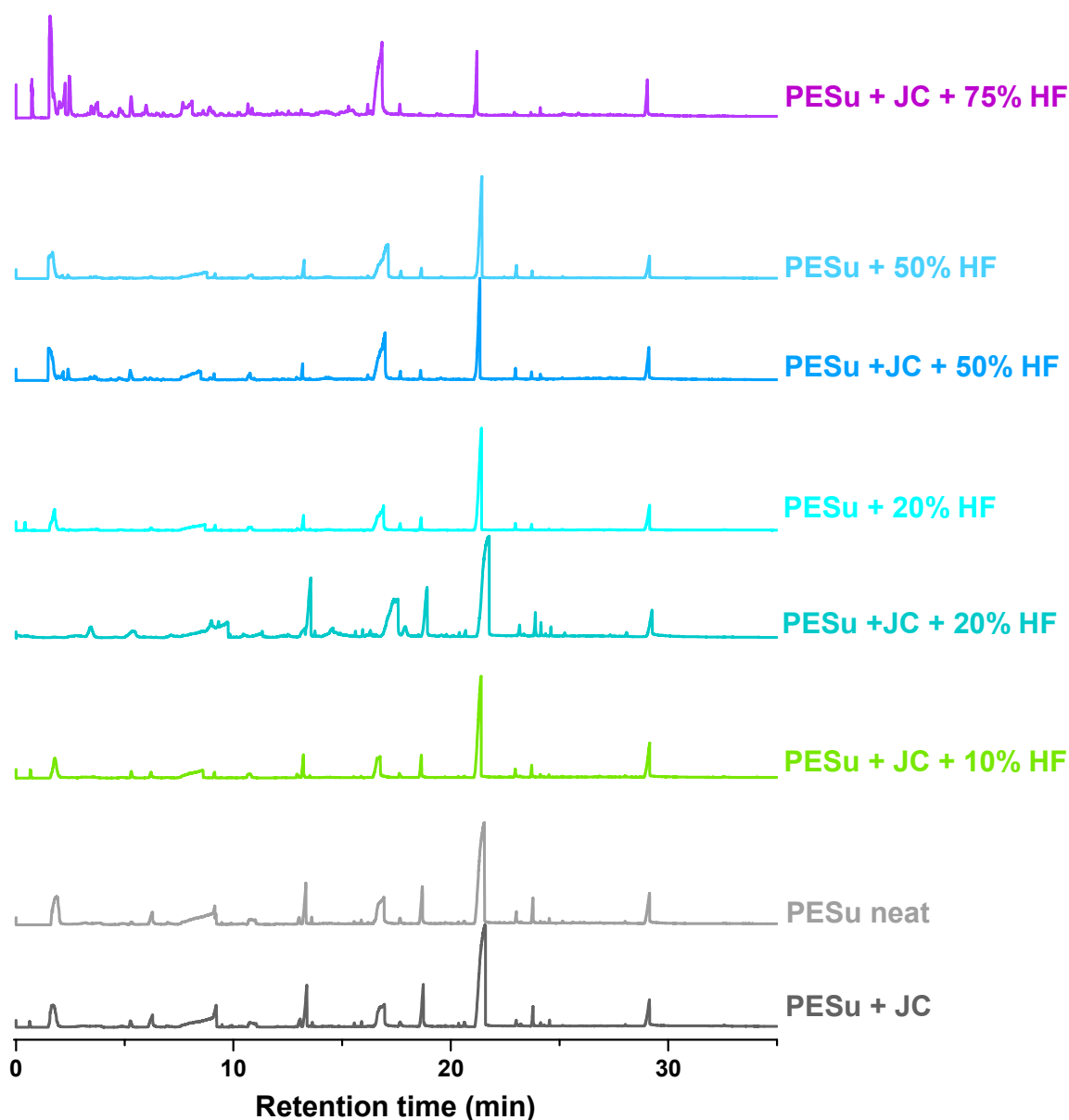


Figure 7. Total ion chromatograms (TICs) of neat PESu, and PESu composites with hemp fibers with/without the incorporation of compatibilizer, pyrolyzed at 450 °C.

Table 3. Thermal decomposition products of neat PESu and PESu composites with hemp fibers.

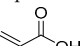
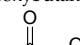
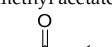
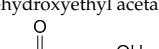
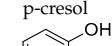
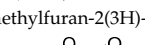
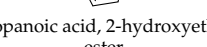

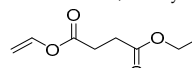
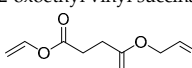
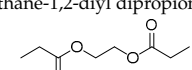
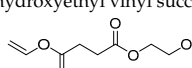
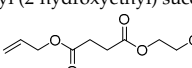
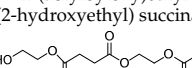
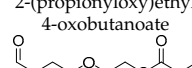
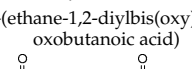
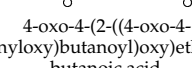
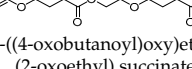
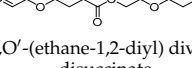
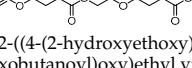
Rt (min)	Sample Name								Mw (amu)	Assigned Compound
	PESu + JC	PESu neat	PESu + JC + 10% HF	PESu + JC + 20% HF	PESu + 20% HF	PESu + JC + 50% HF	PESu + 50% HF	PESu + JC + 75% HF		
	Relative Intensity (%)									
0.6	5.73	-	8.24	2.43	8.02	n.d.	n.d.	38.3	40–44	Carbox dioxide
1.7	21.74	27.46	19.42	1.28	20.36	22.95	25.98	24.79	72	
2.0	n.d.	n.d.	n.d.	n.d.	n.d.	8.82	3.56	16.27	88	1-hydroxybutan-2-one
2.4	n.d.	n.d.	n.d.	2.21	n.d.	11.32	3.8	41.08	74	
3.7	n.d.	n.d.	n.d.	n.d.	n.d.	4.24	2.01	15.61	102	2-hydroxyethyl acetate
4.4	n.d.	n.d.	n.d.	n.d.	n.d.	n.d.	n.d.	6.18	108	
6.0	n.d.	n.d.	n.d.	n.d.	n.d.	n.d.	n.d.	12.5	98	5-methylfuran-2(3H)-one
6.3	12.3	12.57	6.03	1.21	2.98	2.71	2.32	3.87	100	
8.6	n.d.	n.d.	n.d.	n.d.	n.d.	n.d.	n.d.	7.85	124	2-methoxy-phenol (o-Guaiacol)
9.2	21.84	18.43	6.01	16.72	5.43	7.11	5.24	5.28	114	
10.7	4.57	5.36	3.96	4.36	3.44	7.32	3.62	14.23	143	4-oxo-4-(vinylloxy)butanoic acid
11.9	n.d.	n.d.	n.d.	n.d.	n.d.	n.d.	n.d.	7.06	150	
12.5	n.d.	n.d.	n.d.	n.d.	n.d.	n.d.	n.d.	7.01	154	2,6-dimethoxy-phenol (syringol)
13.1	8.31	7.29	6.38	9.74	2.17	16.48	2.24	8.52	158	
13.3	41.35	40.92	23.08	59.08	14.96	1.58	17.89	4.27	160	4-(2-hydroxyethoxy)-4-oxobutanoic acid
13.6	5.01	7.6	2.37	3.81	1.6	1.44	n.d.	4.11	160	

Table 3. Cont.

Rt (min)	Sample Name								Mw (amu)	Assigned Compound
	PESu + JC	PESu neat	PESu + JC + 10% HF	PESu + JC + 20%HF	PESu + 20% HF	PESu + JC + 50% HF	PESu + 50% HF	PESu + JC + 75% HF		
	Relative Intensity (%)									
15.5	4.52	3.27	1.59	2.63	n.d.	1.8	n.d.	7.89	172	Butanedioic acid, diethyl ester 
15.9	5.80	4.87	1.07	8.76	1.12	1.97	1.42	3.83	186	2-oxoethyl vinyl succinate 
16.9	22.59	27.1	21.4	38.2	24.66	46.88	32.84	74.19	174	ethane-1,2-diyl dipropionate 
17.6	5.31	6.60	4.96	11.53	6.94	9.38	7.61	13.78	189	2-hydroxyethyl vinyl succinate 
18.7	42.02	37.02	22.28	49.68	12.27	10.32	10.4	4.87	201	Allyl (2-hydroxyethyl) succinate 
20.3	3.92	3.00	1.79	5.81	n.d.	1.58	n.d.	2.7	258	2-(acryloyloxy)ethyl (2-hydroxyethyl) succinate 
20.6	5.01	3.44	2.01	7.81	n.d.	1.37	n.d.	2.65	202	2-(propionyloxy)ethyl 4-oxobutanoate 
21.5	100	100	100	100	100	100	100	65.12	262	4,4'-(ethane-1,2-diylbis(oxy))bis(4-oxobutanoic acid) 
23.0	7.11	23.96	9.12	13.13	6.7	12.15	13	5.8	289	4-oxo-4-(2-((4-oxo-4-(vinylloxy)butanoyl)oxy)ethoxy)butanoic acid 
23.7	20.59	26.4	12.73	25.19	6.29	8.97	7.47	5.96	288	2-((4-oxobutanoyl)oxy)ethyl (2-oxoethyl) succinate 
24.1	4.78	3.62	3.89	15.55	n.d.	6.17	1.5	10.59	312	O,O'-(ethane-1,2-diyl) divinyl disuccinate 
29.1	27.1	30.7	34.38	27.85	24.97	32.67	22.03	37.68	333	2-((4-(2-hydroxyethoxy)-4-oxobutanoyl)oxy)ethyl vinyl succinate 

* n.d. accounts for no detected compounds.

The detected compounds display a variety of different structures which could be classified into vinyl-, hydroxyl-, methyl-, carboxyl-, and aldehyde-terminated groups (indicative structures and corresponding mass spectra are displayed in Figure 8). At small retention times (Rt), volatile molecules of lower molecular weights, such as carbon dioxide and 2-propenoic acid are detected. The formation of carbon dioxide is a sign that homolytic processes occur as well as decarboxylation of -COOH end groups of the studied composite materials [56,57]. As the Rt increases, compounds with larger and more complex polymeric structures are identified. At first glance, the majority of the detected peaks are

carboxyl- and vinyl-terminated groups, such as 2-propenoic acid ($R_t = 1.7$ min), 4-oxo-4-(vinylloxy)butanoic acid ($R_t = 10.7$ min), 4-(allyloxy)-4-oxobutanoic acid ($R_t = 13.1$ min), 4-(2-hydroxyethoxy)-4-oxobutanoic acid ($R_t = 13.3$ min), 4-oxo-4-(2-oxoethoxy)butanoic acid ($R_t = 13.6$ min), butanedioic acid, diethyl ester ($R_t = 15.5$ min), 2-hydroxyethyl vinyl succinate ($R_t = 17.6$ min), allyl (2-hydroxyethyl) succinate ($R_t = 18.7$ min), 4,4'-(ethane-1,2-diylbis(oxy))bis(4-oxobutanoic acid) ($R_t = 21.5$ min), 4-oxo-4-(2-((4-oxo-4-(vinylloxy)butanoyl)oxy)ethoxy)butanoic acid ($R_t = 23.0$ min), and O,O'-(ethane-1,2-diyl) divinyl disuccinate ($R_t = 24.1$ min). In a more limited extent, α -hydrogen bond scission reactions may occur too, forming aldehydes and alcohols, including the following thermally-induced formed products: 2-hydroxyethyl acetate ($R_t = 3.7$ min), 4-(2-hydroxyethoxy)-4-oxobutanoic acid ($R_t = 13.3$ min), 4-oxo-4-(2-oxoethoxy)butanoic acid ($R_t = 13.6$ min), 2-oxoethyl vinyl succinate ($R_t = 15.9$ min), 2-hydroxyethyl vinyl succinate ($R_t = 17.6$ min), allyl (2-hydroxyethyl) succinate ($R_t = 18.7$ min), 2-(acryloyloxy)ethyl (2-hydroxyethyl) succinate ($R_t = 20.3$ min), 2-(propionyloxy)ethyl 4-oxobutanoate ($R_t = 20.6$ min), 2-((4-oxobutanoyl)oxy)ethyl (2-oxoethyl) succinate ($R_t = 23.7$ min), and 2-((4-(2-hydroxyethoxy)-4-oxobutanoyl)oxy)ethyl vinyl succinate ($R_t = 29.1$ min). The latter compounds displayed peaks with smaller relative peak area (%) compared to the β -hydrogen scission products, and thus were recorded in smaller amounts. However, the hydroxyl-terminated products could be derivatives from both hydrolysis reactions of β -scission compounds and α -hydrogen scissions which are favored to a more limited extent over β -scission reactions. Among all the detected pyrolysis products, only four compounds were identified as aldehydes for $R_t = 13.6$, 15.9, 20.6, and 23.7 min, with a relatively small release amount. To the best of our knowledge, the mechanism of PESu thermal degradation was firstly illustrated by our team [55].

Concerning the overall profile of the thermal degradation of the studied materials, the composites with the lower content of hemp fibers display an almost identical profile to neat PESu; a fact attributed to the same chemical structure of the decomposing material, since PESu is the main polymeric matrix. Additionally, as indicated in Table 3, the majority of the assigned degradation products for neat PESu and PESu/hemp fibers composites, with or without the incorporation of the compatibilizer are vinyl- and carboxyl- terminated groups compounds, which are products of the main scission pathway that generally takes place in the degradation of polyesters. Nevertheless, regarding the quantity of the formed pyrolysis products, a slightly fluctuating behavior can be remarked, without a clear trend.

As an overall remark, the main degradation product for almost all the studied samples is found at $R_t = 21.5$ min and is attributed to 2-((4-(2-hydroxyethoxy)-4-oxobutanoyl)oxy)ethyl vinyl succinate, with the exception of the sample with the higher content of hemp fibers filler (PESu + JC + 75% HF), in which the main degradation peak for its TIC is detected at $R_t = 1.56$ min, assigned to carbon dioxide. The latter fact could be attributed to the higher content in carbon compounds of lower molecular weight compared to the higher Mw polymeric chains of PESu due to the prevalence of hemp fibers.

A more complex decomposition profile is observed for the composite with 75% wt. HF, as shown by the greater number of peaks in the TICs presented in Figure 7, recorded after pyrolysis at 450 °C. Newly-formed products can be detected for relatively low retention times, such as $R_t = 2.0$, 2.4, 3.7, 4.4, 6.0, 8.6, 11.9 and 12.5 min, attributed to the thermal degradation derivatives of hemp counterpart, since the latter mentioned filler is rich in cellulose (53–91% *w/w*) and other lignocellulosic compounds (4–18% *w/w* hemicellulose, 1–21% *w/w* lignin and 1–17% pectin) [58,59]. Apart from small ester (2-hydroxyethyl acetate, methyl acetate) and furan (5-methylfuran-2(3H)-one) compounds attributed to the cellulose counterparts, hydroxyphenolics, guaiacyl and syringyl compounds can be also detected (indicative mass spectra are displayed in Figure 9). The appearance of the latter is mainly connected to the thermally induced degradation of the lignocellulosic compounds of hemp. Concerning the specific composite, it should also be noted that the release of lower molecular weight compounds is favored, while the formation of compounds with longer molecular chain displays a decreasing tendency. As aforementioned, this fact can be

attributed to the higher content in lower molecular weight lignocellulosic compounds for the PESu + JC + 75% HF composite material.

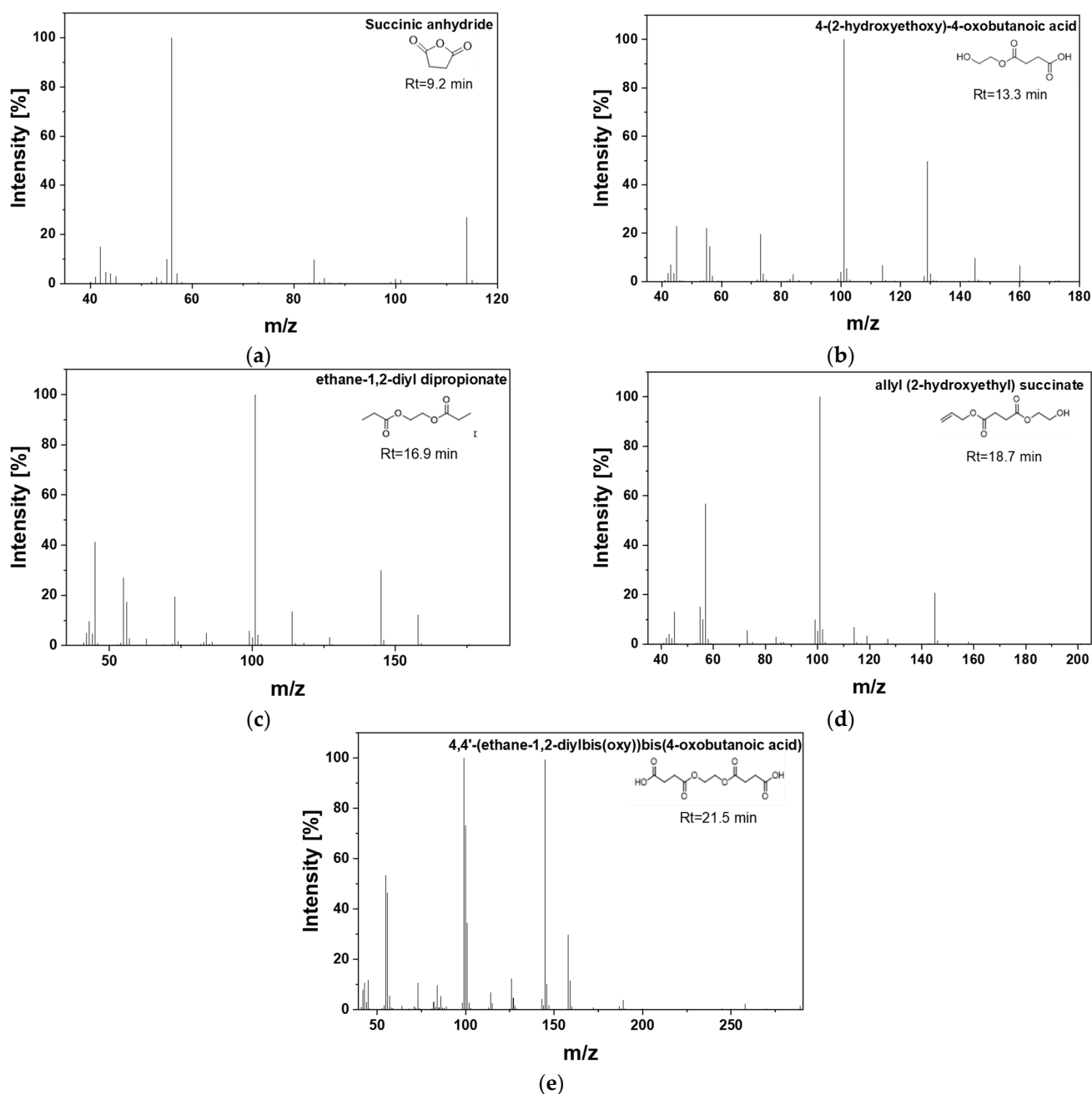


Figure 8. Typical mass spectra of the major decomposition products of PESu composites: (a) succinic anhydride, (b) 4-(2-hydroxyethoxy)-4-oxobutanoic acid, (c) ethane-1,2-diyl dipropionate, (d) allyl (2-hydroxyethyl) succinate, (e) 4,4'-(ethane-1,2-diylbis(oxy))bis(4-oxobutanoic acid).

In the light of the above, it can be concluded that the main thermal degradation pathway for the PESu composites according to Py-GC/MS analysis, is the β -hydrogen scission of the polymeric backbone, since the majority of the detected compounds are vinyl- and carboxyl-ended molecules. An important fact that should be additionally underlined about β -hydrogen scission reactions is the formation of a carbonyl-containing intermediate that can further participate in the degradation reactions through autocatalysis. The autocatalytic nature of the Cn model can arise from the presence of such reactive intermediates that can accelerate the degradation process by catalyzing further decomposition. Thus, the

identification of the β -hydrogen scission mechanism by Py-GC/MS and the autocatalytic Cn model from TGA analysis suggest that the degradation of PESu/hemp fiber composites may involve the formation of reactive intermediates that promote the degradation through autocatalysis. On the other hand, homolytic α -hydrogen bond scission also takes place for both neat PESu and its composites, though to a more limited extent. The composite with the higher amount of hemp fibers presented a slightly different degradation pathway since the profile of the released compounds was differentiated in comparison with the other studied materials, suggesting the impact of lignocellulosic compounds' presence on the degradation profile of the composite. Overall, Py-GC/MS experiments exemplified the outcomes of TGA analysis, as the thermal degradation reactions were proved by slight differences in the releasing decomposition compounds.

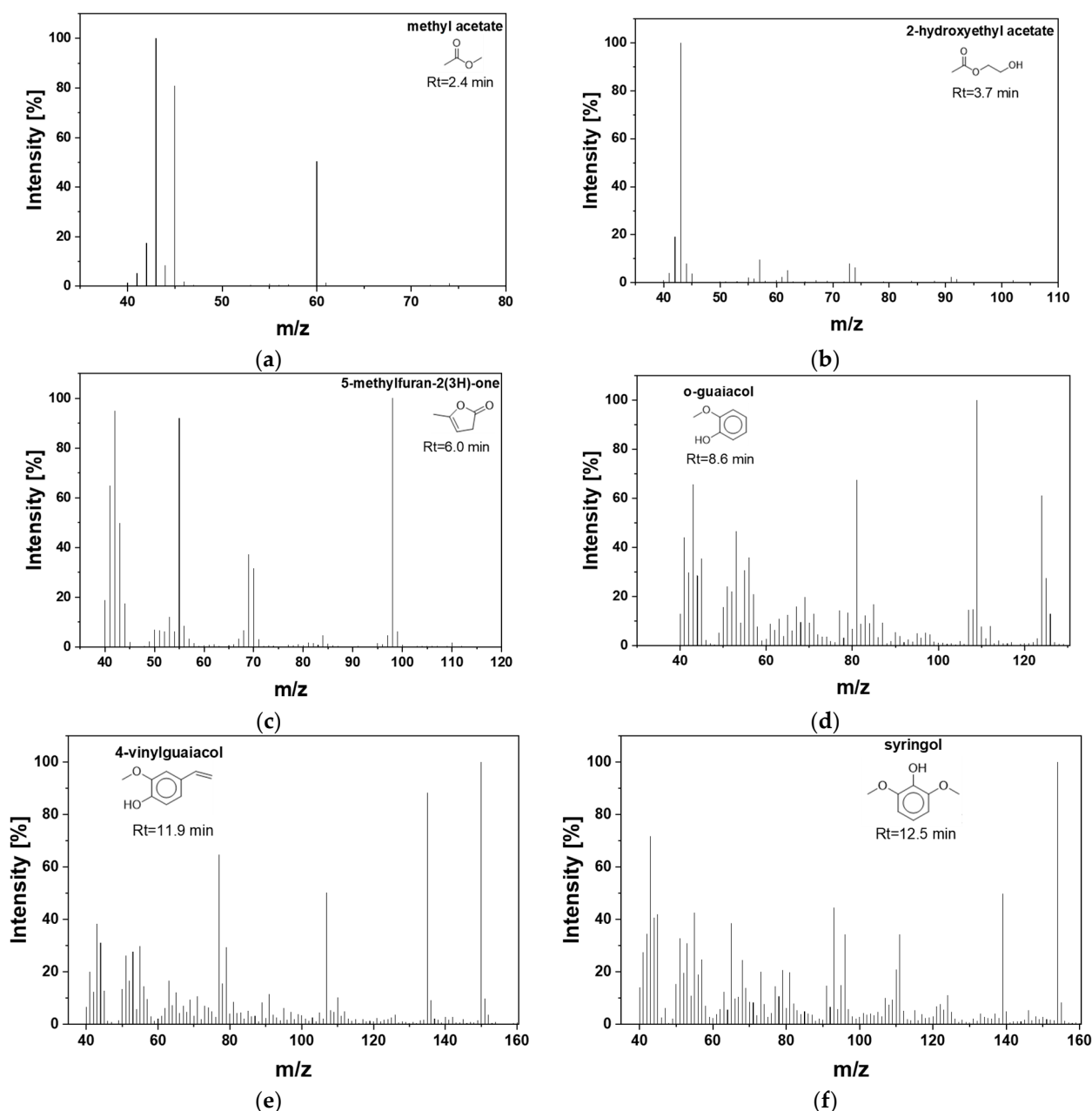


Figure 9. Typical mass spectra of PESu/hemp fibers composites with the higher content in the filler: (a) methyl acetate, (b) 2-hydroxyethyl acetate, (c) 5-methylfuran-2(3H)-one, (d) o-guaiacol, (e) 4-vinylguaiacol, (f) syringol.

4. Conclusions

This study investigates the thermal degradation process of poly(ethylene succinate)-hemp fiber composites. The degradation mechanisms and decomposition products were analyzed using thermogravimetric analysis (TGA) in combination with pyrolysis-gas chromatography/mass spectrometry (Py-GC/MS). Composites with 10, 20, 50 and 75% wt. in HF were prepared as potential alternatives to conventional WPC materials. Joncryl ADR-4400 (JC) was used to enhance the adhesion between the fibers and the polymer matrix. Additionally, composites with 20% and 50% wt. HF were made without JC for comparison.

TGA results indicate that hemp fiber content has the greatest effect on the composites' degradation. As the HF content increases, two degradation steps occur, with the first attributed to hemp fiber and specifically the degradation of cellulosic compounds such as hemicellulose, pectin, and cellulose. The second step corresponds to the degradation of both PESu and hemp (hemicellulose, pectin, cellulose, and lignin). From the comparative thermograms between the samples with and without JC, no significant differences were observed. For the degradation mechanism study, PESu and PESu with 20% wt. HF were chosen. Isoconversional and model-free methods gave precise results, revealing a two-step mechanism for samples without JC and a three-step mechanism for those with JC. The autocatalytic Cn model was used for both cases. Regarding Py-GC/MS analysis, it can be concluded that the main thermal degradation pathway of the PESu/hemp fiber composites is the β -hydrogen scission of the polymeric backbone, with homolytic α -hydrogen bond scission occurring to a lesser extent.

Overall, this study gave us useful information about the thermal degradation of the composites, and it can be assumed that PESu/hemp fiber composites are promising candidates for sustainable polymer applications. Our next goal is to evaluate the mechanical properties of the produced materials as well as their biodegradation rate in the environment compared to conventional non-biodegradable polymers and other wood plastic composites.

Author Contributions: Conceptualization, I.C. and N.M.A.; methodology, I.C. and N.M.A.; software, I.C.; validation, I.C., N.M.A. and E.X.; formal analysis, I.C., N.M.A. and E.X.; investigation, I.C., N.M.A. and E.X.; resources, D.N.B.; data curation, I.C. and N.M.A.; writing—original draft preparation, I.C. and N.M.A.; writing—review and editing, E.X. and A.Z.; visualization, I.C.; supervision, A.Z. and D.N.B.; project administration, D.N.B.; funding acquisition, D.N.B. All authors have read and agreed to the published version of the manuscript.

Funding: This research has been co-financed by the European Union and Greek national funds through the Operational Program Competitiveness, Entrepreneurship and Innovation, under the call RE-SEARCH-CREATE-INNOVATE (project code: T2EDK-00008).

Conflicts of Interest: The authors declare no conflict of interest.

References

1. Hoelscher, F.; Cardoso, P.B.; Candiotti, G.; Guindani, C.; Feuser, P.; Araújo, P.H.H.; Sayer, C. In Vitro Degradation and Cytotoxicity Response of Biobased Nanoparticles Prepared by Thiol-Ene Polymerization in Miniemulsion. *J. Polym. Environ.* **2021**, *29*, 3668–3678. [\[CrossRef\]](#)
2. He, Z.; Feng, Y.; Wang, C.; Yang, J.; Tan, T.; Yang, J. Structure and Properties of New Biodegradable Elastomers Composed of Poly(Ethylene Succinate)-Based Poly(Ether Ester)s and Poly(Lactic Acid). *J. Appl. Polym. Sci.* **2023**, *140*, 1–15. [\[CrossRef\]](#)
3. Keridou, I.; Franco, L.; del Valle, L.J.; Martínez, J.C.; Funk, L.; Turon, P.; Puiggali, J. Hydrolytic and Enzymatic Degradation of Biobased Poly(4-Hydroxybutyrate) Films. Selective Etching of Spherulites. *Polym. Degrad. Stab.* **2021**, *183*, 109451. [\[CrossRef\]](#)
4. Rowe, M.D.; Eyiler, E.; Walters, K.B. Hydrolytic Degradation of Bio-Based Polyesters: Effect of PH and Time. *Polym. Test.* **2016**, *52*, 192–199. [\[CrossRef\]](#)
5. Lv, X.; Luo, F.; Zheng, L.; Niu, R.; Liu, Y.; Xie, Q.; Song, D.Q.; Zhang, Y.C.; Zhou, T.; Zhu, S. Biodegradable Poly(Butylene Succinate-Co-Butylene Furandicarboxylate): Effect of Butylene Furandicarboxylate Unit on Thermal, Mechanical, and Ultraviolet Shielding Properties, and Biodegradability. *J. Appl. Polym. Sci.* **2022**, *139*, e53122. [\[CrossRef\]](#)
6. Burelo, M.; Gutiérrez, S.; Treviño-Quintanilla, C.D.; Cruz-Morales, J.A.; Martínez, A.; López-Morales, S. Synthesis of Biobased Hydroxyl-Terminated Oligomers by Metathesis Degradation of Industrial Rubbers SBS and PB: Tailor-Made Unsaturated Diols and Polyols. *Polymers* **2022**, *14*, 4973. [\[CrossRef\]](#)
7. Chen, S.; Zou, R.; Li, L.; Shang, J.; Lin, S.; Lan, J. Preparation of Biobased Poly(Propylene 2,5-Furandicarboxylate) Fibers: Mechanical, Thermal and Hydrolytic Degradation Properties. *J. Appl. Polym. Sci.* **2021**, *138*. [\[CrossRef\]](#)

8. Arif, Z.U.; Khalid, M.Y.; Sheikh, M.F.; Zolfagharian, A.; Bodaghi, M. Biopolymeric Sustainable Materials and Their Emerging Applications. *J. Environ. Chem. Eng.* **2022**, *10*, 108159. [\[CrossRef\]](#)
9. Papadimitriou, S.A.; Papageorgiou, G.Z.; Bikiaris, D.N. Crystallization and Enzymatic Degradation of Novel Poly (ε-Caprolactone-Co-Propylene Succinate) Copolymers. *Eur. Polym. J.* **2008**, *44*, 2356–2366. [\[CrossRef\]](#)
10. Papageorgiou, D.G.; Roumeli, E.; Chrissafis, K.; Lioutas, C.; Triantafyllidis, K.; Bikiaris, D.; Boccaccini, A.R. Thermal Degradation Kinetics and Decomposition Mechanism of PBSu Nanocomposites with Silica-Nanotubes and Strontium Hydroxyapatite Nanorods. *Phys. Chem. Chem. Phys.* **2014**, *16*, 4830–4842. [\[CrossRef\]](#)
11. Lv, X.; Haitao, L.; Zhengxiang, W.; Ruixue, N.; Yi, L.; Wei, Y.; Zheng, L. Synthesis of Biodegradable Polyester–Polyether with Enhanced Hydrophilicity, Thermal Stability, Toughness, and Degradation Rate. *Polymers* **2022**, *14*, 4895. [\[CrossRef\]](#) [\[PubMed\]](#)
12. Bikiaris, R.D.; Ainali, N.M.; Christodoulou, E.; Nikolaidis, N.; Lambropoulou, D.A.; Papageorgiou, G.Z. Thermal Stability and Decomposition Mechanism of Poly(Alkylene Succinate)S. *Macromol* **2022**, *2*, 58–77. [\[CrossRef\]](#)
13. Bikiaris, D.N.; Achilias, D.S. Synthesis of Poly(Alkylene Succinate) Biodegradable Polyesters, Part II: Mathematical Modelling of the Polycondensation Reaction. *Polymer* **2008**, *49*, 3677–3685. [\[CrossRef\]](#)
14. Chrissafis, K.; Paraskevopoulos, K.M.; Bikiaris, D.N. Thermal Degradation Mechanism of Poly (Ethylene Succinate) and Poly (Butylene Succinate): Comparative Study. *Thermochim. Acta* **2005**, *435*, 142–150. [\[CrossRef\]](#)
15. Bikiaris, D.; Prinos, J.; Panayiotou, C. Effect of EAA and Starch on the Thermooxidative Degradation of LDPE. *Polym. Degrad. Stab.* **1997**, *56*, 1–9. [\[CrossRef\]](#)
16. Burgada, F.; Fages, E.; Quiles-Carrillo, L.; Lascano, D.; Ivorra-Martinez, J.; Arrieta, M.P.; Fenollar, O. Upgrading Recycled Polypropylene from Textile Wastes in Wood Plastic Composites with Short Hemp Fiber. *Polymers* **2021**, *13*, 1248. [\[CrossRef\]](#)
17. Dolça, C.; Fages, E.; Gong, E.; Garcia-sanoguera, D.; Balart, R.; Quiles-carrillo, L. The Effect of Varying the Amount of Short Hemp Fibers on Mechanical and Thermal Properties of Wood–Plastic Composites from Biobased Polyethylene Processed by Injection Molding. *Polymers* **2022**, *14*, 138. [\[CrossRef\]](#)
18. Väisänen, T.; Batello, P.; Lappalainen, R.; Tomppo, L. Modification of Hemp Fibers (*Cannabis Sativa* L.) for Composite Applications. *Ind. Crops Prod.* **2018**, *111*, 422–429. [\[CrossRef\]](#)
19. Xanthopoulou, E.; Chrysafi, I.; Polychronidis, P.; Zamboulis, A.; Bikiaris, D.N. Evaluation of Eco-Friendly Hemp-Fiber-Reinforced Recycled HDPE Composites. *J. Compos. Sci.* **2023**, *7*, 138. [\[CrossRef\]](#)
20. Marcuello, C.; Chabbert, B.; Berzin, F.; Bercu, N.B.; Molinari, M. Influence of Surface Chemistry of Fiber and Lignocellulosic Materials on Adhesion Properties with Polybutylene Succinate at Nanoscale. *Materials* **2023**, *16*, 2440. [\[CrossRef\]](#)
21. Lostao, A.; Lim, K.S.; Pallarés, M.C.; Ptak, A.; Marcuello, C. Recent Advances in Sensing the Inter-Biomolecular Interactions at the Nanoscale—A Comprehensive Review of AFM-Based Force Spectroscopy. *Int. J. Biol. Macromol.* **2023**, *238*, 124089. [\[CrossRef\]](#) [\[PubMed\]](#)
22. Dolza, C.; Gong, E.; Fages, E.; Tejada-Oliveros, R.; Balart, R.; Quiles-Carrillo, L. Green Composites from Partially Bio-Based Poly(Butylene Succinate-Co-Adipate)-PBSA and Short Hemp Fibers with Itaconic Acid-Derived Compatibilizers and Plasticizers. *Polymers* **2022**, *14*, 1968. [\[CrossRef\]](#) [\[PubMed\]](#)
23. Tanasă, F.; Zănoagă, M.; Teacă, C.A.; Nechifor, M.; Shahzad, A. Modified Hemp Fibers Intended for Fiber-Reinforced Polymer Composites Used in Structural Applications—A Review. I. Methods of Modification. *Polym. Compos.* **2020**, *41*, 5–31. [\[CrossRef\]](#)
24. Ashori, A. Wood-Plastic Composites as Promising Green-Composites for Automotive Industries! *Bioresour. Technol.* **2008**, *99*, 4661–4667. [\[CrossRef\]](#)
25. Manaia, J.P.; Manaia, A.T.; Rodrigues, L. Industrial Hemp Fibers: An Overview. *Fibers* **2019**, *7*, 106. [\[CrossRef\]](#)
26. Scarponi, C.; Messano, M. Comparative Evaluation between E-Glass and Hemp Fiber Composites Application in Rotorcraft Interiors. *Compos. B Eng.* **2015**, *69*, 542–549. [\[CrossRef\]](#)
27. Sathish, T.; Palani, K.; Natrayan, L.; Merneedi, A.; de Pours, M.V.; Singaravelu, D.K. Synthesis and Characterization of Polypropylene/Ramie Fiber with Hemp Fiber and Coir Fiber Natural Biopolymer Composite for Biomedical Application. *Int. J. Polym. Sci.* **2021**, *2021*, 2462873. [\[CrossRef\]](#)
28. Ticoalu, A.; Aravinthan, T.; Cardona, F. A Review of Current Development in Natural Fiber Composites in Automotive Applications. *Appl. Mech. Mater.* **2010**, *564*, 3–7. [\[CrossRef\]](#)
29. Awwad, E.; Mabsout, M.; Hamad, B.; Farran, M.T.; Khatib, H. Studies on Fiber-Reinforced Concrete Using Industrial Hemp Fibers. *Constr. Build. Mater.* **2012**, *35*, 710–717. [\[CrossRef\]](#)
30. Abu-Saleem, M.; Zhuge, Y.; Hassanli, R.; Ellis, M.; Rahman, M.; Levett, P. Evaluation of Concrete Performance with Different Types of Recycled Plastic Waste for Kerb Application. *Constr. Build. Mater.* **2021**, *293*, 123477. [\[CrossRef\]](#)
31. Tran Le, A.D.; Maalouf, C.; Mai, T.H.; Wurtz, E.; Collet, F. Transient Hygrothermal Behaviour of a Hemp Concrete Building Envelope. *Energy Build.* **2010**, *42*, 1797–1806. [\[CrossRef\]](#)
32. Shahzad, A. Hemp Fiber and Its Composites—A Review. *J. Compos. Mater.* **2012**, *46*, 973–986. [\[CrossRef\]](#)
33. Fang, H.; Zhang, Y.; Deng, J.; Rodrigue, D. Effect of Fiber Treatment on the Water Absorption and Mechanical Properties of Hemp Fiber/Polyethylene Composites. *J. Appl. Polym. Sci.* **2013**, *127*, 942–949. [\[CrossRef\]](#)
34. Panaitescu, D.M.; Fierascu, R.C.; Gabor, A.R.; Nicolae, C.A. Effect of Hemp Fiber Length on the Mechanical and Thermal Properties of Polypropylene/SEBS/Hemp Fiber Composites. *J. Mater. Res. Technol.* **2020**, *9*, 10768–10781. [\[CrossRef\]](#)
35. Zhao, J.; Wang, X.; Zhou, W.; Zhi, E.; Zhang, W.; Ji, J. Graphene-Reinforced Biodegradable Poly(Ethylene Succinate) Nanocomposites Prepared by In Situ Polymerization. *J. Appl. Polym. Sci.* **2013**, *130*, 3212–3220. [\[CrossRef\]](#)

36. Rafiqah, S.A.; Khalina, A.; Harmaen, A.S.; Tawakkal, I.A.; Zaman, K.; Asim, M.; Nurrazi, M.N.; Lee, C.H. A Review on Properties and Application of Bio-based Poly(Butylene Succinate). *Polymers* **2021**, *13*, 1436. [\[CrossRef\]](#)
37. Bikiaris, D.N.; Chrissafis, K.; Paraskevopoulos, K.M.; Triantafyllidis, K.S.; Antonakou, E.V. Investigation of Thermal Degradation Mechanism of an Aliphatic Polyester Using Pyrolysis-Gas Chromatography-Mass Spectrometry and a Kinetic Study of the Effect of the Amount of Polymerisation Catalyst. *Polym. Degrad. Stab.* **2007**, *92*, 525–536. [\[CrossRef\]](#)
38. Chrissafis, K.; Paraskevopoulos, K.M.; Bikiaris, D.N. Effect of Molecular Weight on Thermal Degradation Mechanism of the Biodegradable Polyester Poly(Ethylene Succinate). *Thermochim. Acta* **2006**, *440*, 166–175. [\[CrossRef\]](#)
39. Klonos, P.A.; Papadopoulos, L.; Kasimatis, M.; Iatrou, H.; Kyritsis, A.; Bikiaris, D.N. Synthesis, Crystallization, Structure Memory Effects, and Molecular Dynamics of Biobased and Renewable Poly (n-Alkylene Succinate)s with n from 2 to 10. *Macromolecules* **2021**, *54*, 1106–1119. [\[CrossRef\]](#)
40. Asimakidou, T.; Chrissafis, K. Thermal Behavior and Pyrolysis Kinetics of Olive Stone Residue. *J. Therm. Anal. Calorim.* **2022**, *147*, 9045–9054. [\[CrossRef\]](#)
41. Hamadache, H.; Djidjelli, H.; Boukerrou, A.; Kaci, M.; José Antonio, J.R.; Martín-Martínez, J.M. Different Compatibility Approaches to Improve the Thermal and Mechanical Properties of EVA/Starch Composites. *Polym. Compos.* **2019**, *40*, 3242–3253. [\[CrossRef\]](#)
42. Eszer, N.H.; Ishak, Z.A.M. Effect of Compatibilizer on Morphological, Thermal and Mechanical Properties of Starch-Grafted-Polypropylene/Kenaf Fibers Composites. *IOP Conf. Ser. Mater. Sci. Eng.* **2018**, *368*, 012017. [\[CrossRef\]](#)
43. Zoukrami, F.; Haddaoui, N.; Slavons, M.; Devaux, J.; Vanzeveren, C. Rheological Properties and Thermal Stability of Compatibilized Polypropylene/Untreated Silica Composites Prepared by Water Injection Extrusion Process. *Polym. Bull.* **2018**, *75*, 5551–5566. [\[CrossRef\]](#)
44. Kim, H.S.; Kim, S.; Kim, H.J.; Yang, H.S. Thermal Properties of Bio-Flour-Filled Polyolefin Composites with Different Compatibilizing Agent Type and Content. *Thermochim. Acta* **2006**, *451*, 181–188. [\[CrossRef\]](#)
45. Tsanakis, V.; Vouvoudi, E.; Papageorgiou, G.Z.; Papageorgiou, D.G.; Chrissafis, K.; Bikiaris, D.N. Thermal Degradation Kinetics and Decomposition Mechanism of Polyesters Based on 2,5-Furandicarboxylic Acid and Low Molecular Weight Aliphatic Diols. *J. Anal. Appl. Pyrolysis* **2015**, *112*, 369–378. [\[CrossRef\]](#)
46. Vyazovkin, S.; Burnham, A.K.; Criado, J.M.; Pérez-maqueda, L.A.; Popescu, C.; Sbirrazzuoli, N. Thermochemical Acta ICTAC Kinetics Committee Recommendations for Performing Kinetic Computations on Thermal Analysis Data. *Thermochim. Acta* **2011**, *520*, 1–19. [\[CrossRef\]](#)
47. Peterson, J.D.; Vyazovkin, S.; Wight, C.A. Kinetic Study of Stabilizing Effect of Oxygen on Thermal Degradation of Poly(Methyl Methacrylate). *J. Phys. Chem. B* **1999**, *103*, 8087–8092. [\[CrossRef\]](#)
48. Chrissafis, K. Detail Kinetic Analysis of the Thermal Decomposition of PLA with Oxidized Multi-Walled Carbon Nanotubes. *Thermochim. Acta* **2010**, *511*, 163–167. [\[CrossRef\]](#)
49. Vyazovkin, S. Modification of the Integral Isoconversional Method to Account for Variation in the Activation Energy. *J. Comput. Chem.* **2001**, *22*, 178–183. [\[CrossRef\]](#)
50. Vyazovkin, S. Evaluation of Activation Energy of Thermally Stimulated Solid-State Reactions under Arbitrary Variation of Temperature. *J. Comput. Chem.* **1997**, *18*, 393–402. [\[CrossRef\]](#)
51. Levchik, S.V.; Weil, E.D. A Review on Thermal Decomposition and Combustion of Thermoplastic Polyesters. *Polym. Adv. Technol.* **2004**, *15*, 691–700. [\[CrossRef\]](#)
52. Nguyen, S.; Yu, G.; Marchessault, R.H. Thermal Degradation of Poly(3-Hydroxyalkanoates): Preparation of Well-Defined Oligomers. *Biomacromolecules* **2002**, *3*, 219–224. [\[CrossRef\]](#) [\[PubMed\]](#)
53. Atkinson, J.L.; Vyazovkin, S. Thermal Properties and Degradation Behavior of Linear and Branched Poly(L-Lactide)s and Poly(L-Lactide-Co-Glycolide)s. *Macromol. Chem. Phys.* **2012**, *213*, 924–936. [\[CrossRef\]](#)
54. Terzopoulou, Z.; Tsanakis, V.; Nerantzaki, M.; Achilias, D.S.; Vaimakis, T.; Papageorgiou, G.Z.; Bikiaris, D.N. Thermal Degradation of Biobased Polyesters: Kinetics and Decomposition Mechanism of Polyesters from 2,5-Furandicarboxylic Acid and Long-Chain Aliphatic Diols. *J. Anal. Appl. Pyrolysis* **2016**, *117*, 162–175. [\[CrossRef\]](#)
55. Chrissafis, K.; Paraskevopoulos, K.M.; Bikiaris, D. Thermal Degradation Kinetics and Decomposition Mechanism of Two New Aliphatic Biodegradable Polyesters Poly(Propylene Glutarate) and Poly(Propylene Suberate). *Thermochim. Acta* **2010**, *505*, 59–68. [\[CrossRef\]](#)
56. Terzopoulou, Z.; Tsanakis, V.; Nerantzaki, M.; Papageorgiou, G.Z.; Bikiaris, D.N. Decomposition Mechanism of Polyesters Based on 2,5-Furandicarboxylic Acid and Aliphatic Diols with Medium and Long Chain Methylene Groups. *Polym. Degrad. Stab.* **2016**, *132*, 127–136. [\[CrossRef\]](#)
57. Rizzarelli, P.; Carroccio, S. Thermo-Oxidative Processes in Biodegradable Poly(Butylene Succinate). *Polym. Degrad. Stab.* **2009**, *94*, 1825–1838. [\[CrossRef\]](#)
58. Liu, M.; Thygesen, A.; Summerscales, J.; Meyer, A.S. Targeted Pre-Treatment of Hemp Bast Fibres for Optimal Performance in Biocomposite Materials: A Review. *Ind. Crops Prod.* **2017**, *108*, 660–683. [\[CrossRef\]](#)
59. Zimniewska, M. Hemp Fibre Properties and Processing Target Textile: A Review. *Materials* **2022**, *15*, 1901. [\[CrossRef\]](#)

Disclaimer/Publisher’s Note: The statements, opinions and data contained in all publications are solely those of the individual author(s) and contributor(s) and not of MDPI and/or the editor(s). MDPI and/or the editor(s) disclaim responsibility for any injury to people or property resulting from any ideas, methods, instructions or products referred to in the content.